INDUSTRIAL PHOTOCHEMISTRY VII: LIGHT DISTRIBUTION IN A DIFFUSING MEDIUM OF TITANIUM DIOXIDE IN WATER

C. BRAUN and J. C. ANDRE

Groupe de Recherches et Applications en Photophysique et Photochimie, Laboratoire associé au CNRS 328, Ecole Nationale Supérieure des Industries Chimiques — Institut National Polytechnique de Lorraine, 1 rue Grandville, 54042 Nancy Cedex (France)

(Received April 24, 1984)

Summary

The experimental determination of the total light distribution in an aqueous solution of titanium dioxide for an almost non-absorbing wavelength shows that the extinction coefficient exhibits a non-linear dependence on the concentration at high solute concentrations. The axial and radial light distributions, measured relative to an incident light beam of small cross section, are monoexponential and bi-exponential decay functions respectively. The proportion of scattered light relative to the total amount of light incident on an axial cross section is a function which increases exponentially with increasing distance. A computer-run Monte Carlo simulation of multiple diffusion shows the same behaviour.

1. Introduction

In order to develop new photochemical and photoelectrochemical (see for example ref. 1) methods using absorbing semiconductors to a pilot plant stage, a knowledge of the absorption laws in a highly scattering liquid–solid medium is of prime importance to allow us to calculate the optimum dimensions of a reactor [1, 2].

Certain reactions use direct sunlight; this is the case for photosystems adapted to the purification of water [3]. Under such conditions we can consider that the solar source of light behaves in the same way as does a system emitting almost parallel light rays with a uniform luminous flux at the entrance to the reactor represented schematically in Fig. 1. However, to determine the profile of the light distribution in such a scattering medium, it was necessary for us to build a model and to develop an experimental method under easily accessible conditions.

The results of this preliminary study, which show that the concentration of the scattering substance has little influence on the light distribution

0047-2670/85/$3.30

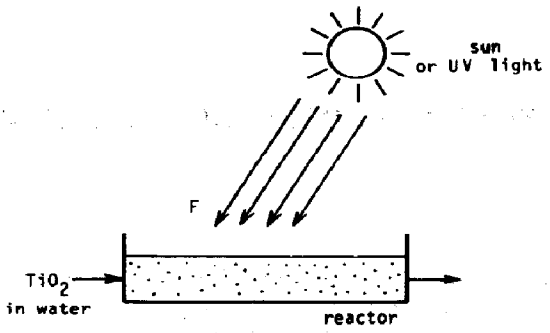

Fig. 1. Photoreactor used for the photoelectrochemical purification of water.

in a semi-infinite reactor (except for back scattering), form the subject of the present paper. They serve as a basis for the study of more complex experimental systems including those in which absorption, the superposition of several wavelengths and the influence of the shape of the reactor, of the spatiotemporal distribution of the solid support and also of the size of the scattering substance must be taken into account.

2. Monte Carlo simulations of the light distribution in a scattering medium

When a system has a sufficiently large volume, which naturally depends on the scattering power of the particles and on their concentration, multiple scattering occurs [4]. As has been mentioned by Ravey [4], the scattering properties of such a system apparently have nothing in common with the properties of the elementary volume, which contains one particle at the most, with respect to the intensities, polarization, angular distribution, absorption etc. The essential effects of multiple scattering are to make the scattering diagrams completely blurred and to increase the intensity of the backscattering significantly.

On the assumption that, in the medium under consideration, we have an isotopic scatterer comprising several independent scatterers in the elementary volume so that the phase function $P(\Omega)$, which describes the angular distribution of the scattered intensity by this element of volume, is independent of the angle Ω between the directions of the incident and the scattered light rays, we carried out a simulation of the light distribution in a reactor schematized in Fig. 2 in which the light enters the face normally. We consider that the light enters by a very small area s (this is what happens when the solution is irradiated with a laser).

If the wavelength of the light is such that the scattering substances do not absorb it, the albedo is equal to unity and we do not have to take it into account in the simulation of the light absorption processes. From the assumptions discussed above, we have therefore assumed that a photon has a probability p (chosen to be equal to 0.1) of being scattered when it enters the elementary volume dV in any direction defined by the angles θ and φ.

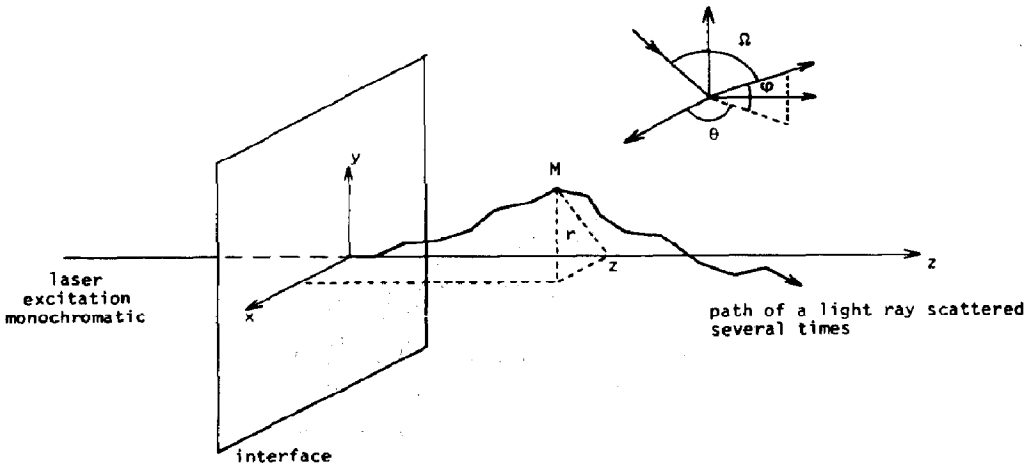

Fig. 2. Schematic representative of the multidiffusional process.

The mean free path was equal to unity and the results were assembled into a matrix of 50 by 50 elements, representing length z and radius r. Every photon leaving the volume of $50 \times 50 \times \pi$ units^2 caused a new photon to enter at 0.0, corresponding to values of r greater than 50 units.

Figures 3 and 4 show the axial and radial distributions in logarithmic units. While the straight line in Fig. 3 corresponds to a simple exponential function, Fig. 4 shows a function of intensity which varies at least bi-exponentially with the radius as in the experiment (see Section 4). Thus in an analytical form the results of these calculations define the signals to be treated. Indeed, only parametric adjustments can be suggested since, to our knowledge, simple and analytical results do not exist even for the most simplified theories.

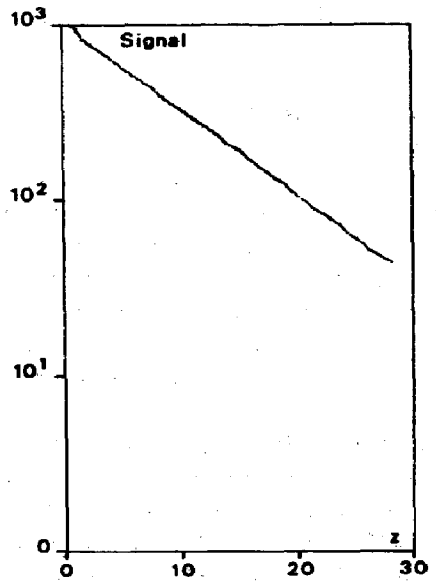

Fig. 3. Semilogarithmic plot of the light distribution at $r = 0$.

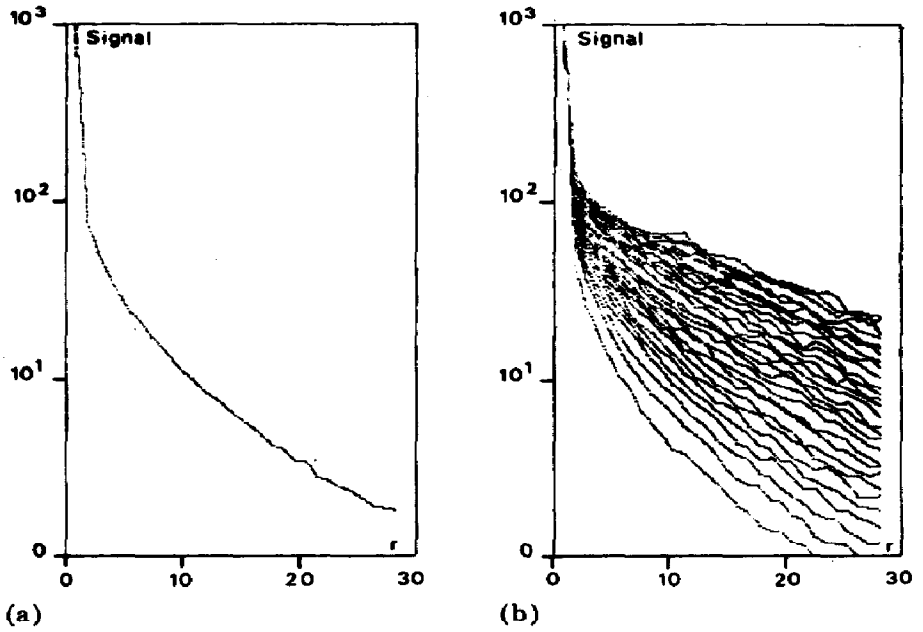

Fig. 4. Semilogarithmic plot of the light distribution: (a) at $z = 4$; (b) with z varying between 0 and 30.

3. Experimental details

As stated in Section 1, we have built a model system comprising the following elements: a monochromatic non-absorbed (albedo of unity) parallel light source of small cross section; a stirred almost semi-infinite closed reactor; a scattering substance titanium dioxide which does not absorb the incident light. The system is represented schematically in Fig. 5.

3.1. Source and reactor

The model system was achieved by means of the following experimental set-up, schematized in Figs. 2 and 5. A laser light beam of cross sectional area 3.1 mm^2 and of wavelength 632.8 nm (Spectraphysics) was reflected vertically into the solution by a mirror. The detector, which could be moved in all directions by means of a mechanical displacing system, transmitted the light through an optical fibre to a monochromator which transmits light at 632.8 nm, a photomultiplier and a subsequent amplification system. The signal was recorded on a strip chart. The solution was kept at a constant temperature of 17 °C by means of a heat exchanger and a stirrer.

In order to measure the total light intensity, regardless of the incident angle, at a given point on the reactor, we fixed an integrating sphere of radius $R = 1.8$ mm at the end of the optical fibre. The sphere was made out of a polymerized dental product (ESPE Visio Bond) [5] and showed a deviation from uniform transmittance over the surface of —1.1% (the constant attenuation factor was not taken into account) (Fig. 6).

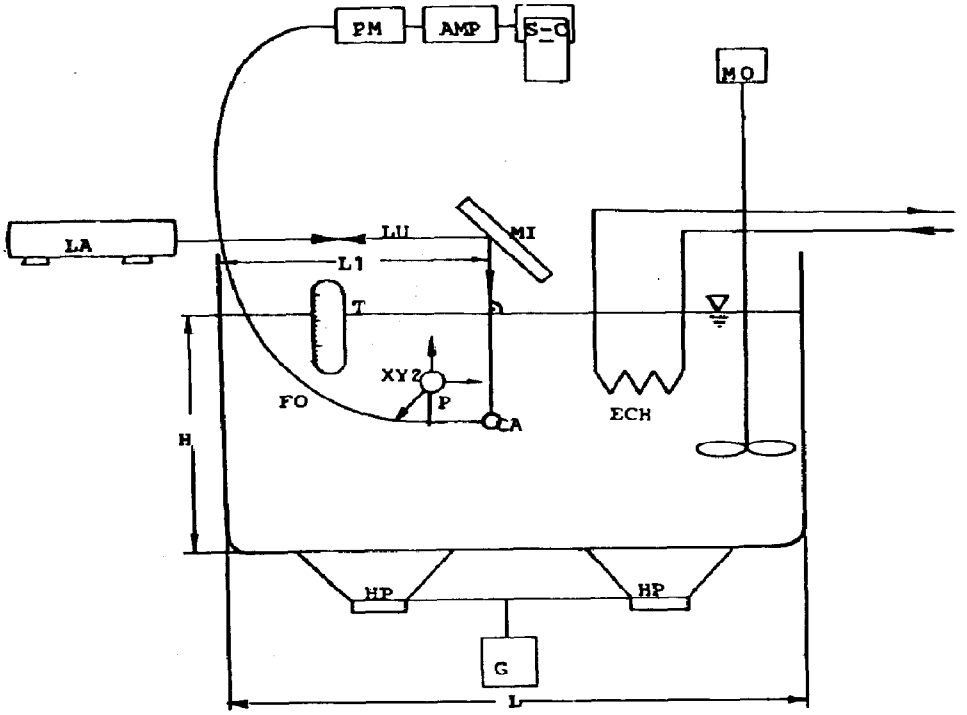

Fig. 5. Diagram of the experimental set-up (H = 90 mm; L = 225 mm; L_1 = 170 mm): AMP, home-made amplifier; CA, detector (see text) (radius, 1.8 mm); ECH, copper heat exchanger; F, optical fibre (diameter, 1 mm); G, ultrasound generator (Ultrasonic NSU157); HP, ultrasonic loud speakers; LA, He–Ne laser (632.8 nm; 6.95 mW); LU, light path; MI, mirror; MO, propeller motor; S, support for the optical fibre; PM, photomultiplier (Hamamatzu IP28) and monochromator (Jobin-Yvon H20) (λ = 632.8 nm); T, thermometer (temperature, 17 °C); SC, strip chart recorder (Sefram); XYZ, displacing system for the detector in the three spatial coordinates.

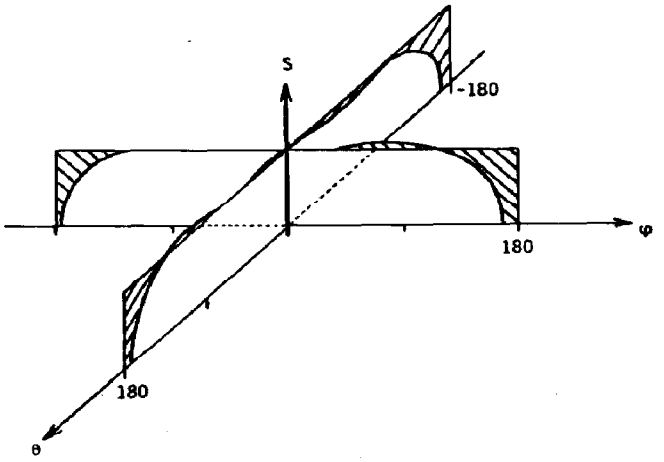

Fig. 6. Response functions for the integrating sphere. The curves represent the transmittance for 632.8 nm as functions of φ and θ. The shaded areas represent overtransmittance or undertransmittance.

Great care was taken in the alignment of the direct light propagation axis and the z axis of our displacing system. Nevertheless, to correct for any possible deviation, for every measuring plane orthogonal to the incident light beam, we positioned the detector at the maximum intensity value and defined this position as $r = 0$ of the plane. The total error in the intensities measured was between −2.6% and +0.3%.

Thus, for a system of restricted size, which eliminates to a maximum degree the shadow effects and which recovers to a significant extent the light at a point of coordinates r, z over 4π sr at our disposal, it is possible to have conditions similar to those defined by the Monte Carlo type of simulations discussed in Section 2.

3.2. Preparation of the mixtures

The titanium dioxide was mainly anatase (Degussa P25). An analysis using a goniodiffusometer, for very dilute concentrations in the linear range, showed a ratio $P(45)/P(135)$ of 5.2. These values correspond to the scatterings at 45° and 135° respectively of the incident light. This in turn leads to a mean radius r of 260 nm or 350 nm for assumed spheres or discs respectively. Thus the ratio $2r/\lambda$, where λ is the excitation wavelength, is at least 0.47.

We prepared five different solutions of titanium dioxide in demineralized water, as shown in Table 1. The wetting of the highly dispersed powder was accomplished by sonification and stirring of the solution. To prevent decantation, which takes place in a few minutes, we maintained an ultrasound treatment throughout the experiment.

TABLE 1

Experimental results

Run	c ($\times 10^{-2}$ g l^{-1})	A (arbitrary units)	B	B_0 (mm^{-1})	F (l g^{-1})	M (arbitrary units)	N (mm^{-1})	$P = MN$ (arbitrary units)
1	4.55	0.977	0.0357			1302	0.019	25
2	9.44	0.985	0.0701					
3	14.47	1.057	0.0984	0.247	0.035	1618	0.019	31
4	18.78	1.026	0.118					
5	23.47	1.054	0.138			1883	0.018	35

The measurements for each concentration were performed over 2 - 3 h and more titanium dioxide was subsequently added to the solution to obtain higher concentrations. The concentrations indicated in Table 1 are corrected for evaporation and sample taking. The ultrasound treatment was not interrupted to prevent partial decantation. The final solution (run 5) was then found to be stable for several weeks. In order to evaluate the importance of

the superposition of Brillouin scattering by ultrasound, the ratio of the velocity of sound to that of light being only $10^{-5} - 10^{-6}$, the intensity measured was no different from that measured when the sound treatment was interrupted in a previous experiment.

4. Results and discussions

4.1. Results for r = 0

For all five solutions, the variation in the light intensity was measured in a plane lying between the axis z of propagation of the incident light beam and the coordinate r orthogonal to z at the surface of the solution. The typical dependence of J on z, for $r = 0$, is shown in Fig. 7. $J(0, z)$ can be represented by the simple exponential as is found for absorption:

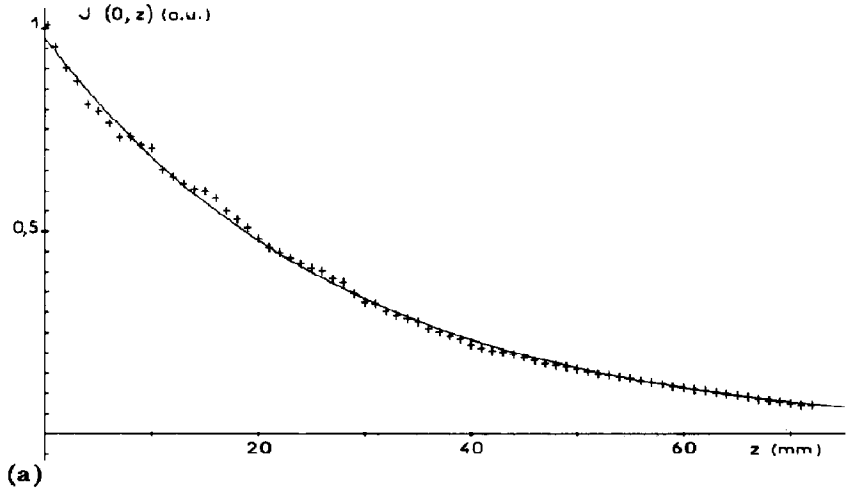

(a)

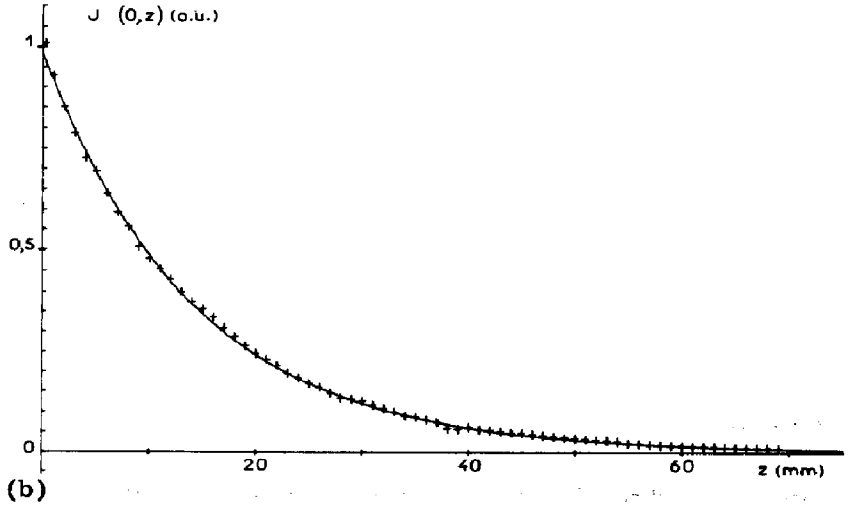

(b)

Fig. 7 ***(continued).***

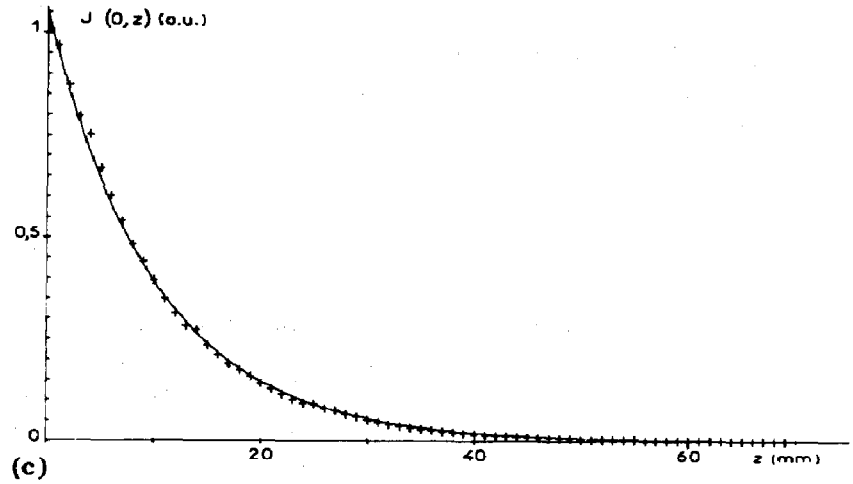

(c)

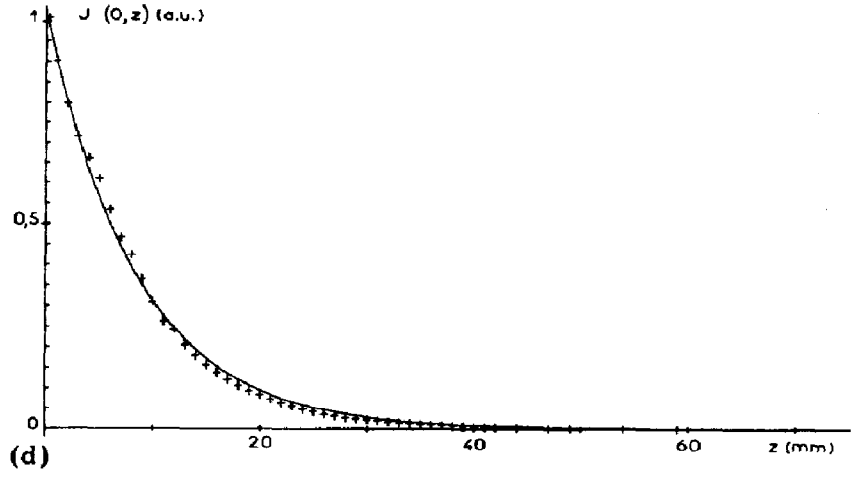

(d)

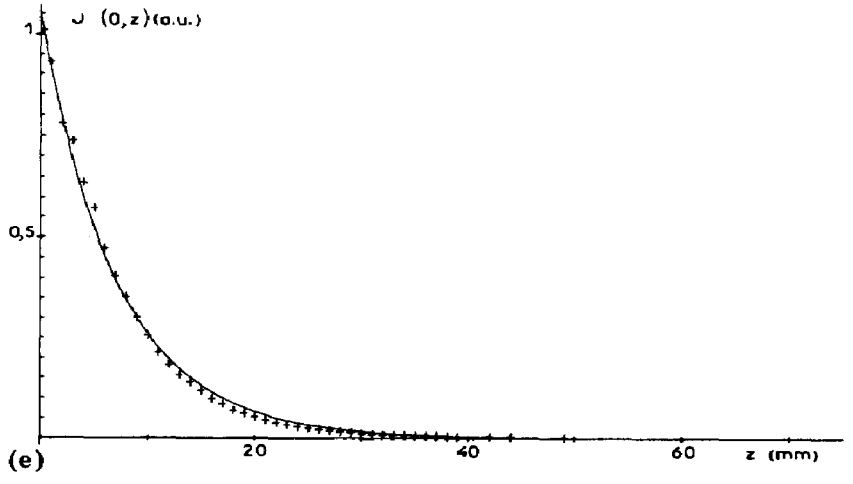

(e)

Fig. 7. Light distribution $J(0, z)$ for (a) run 1, (b) run 2, (c) run 3, (d) run 4 and (e) run 5 (see text and Table 1).

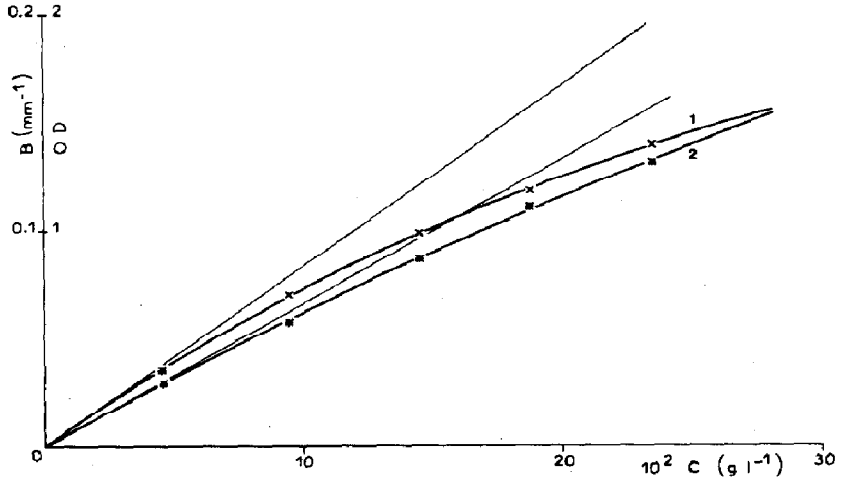

Fig. 8. Variation in B with c (curve 1) and variation in the optical density with the concentration measured on a Cary 15 apparatus (λ = 632.8; cell thickness, 1 cm) (curve 2).

$$J(0, z) = A \exp(-Bz) \tag{1}$$

The different values found for the five concentrations obtained by a least-squares treatment are also shown in Table 1. A representation of the different values of B *versus* the concentration c is shown in Fig. 8, curve 1. B itself is thus a function of c and becomes approximately

$$B = B_0\{1 - \exp(-Fc)\} \tag{2}$$

where B_0 and F are two adjustable values, shown in Table 1. Finally, the axial intensity J as a function of z becomes

$$J(0, z) = A \exp[-zB_0\{1 - \exp(-Fc)\}] \tag{3}$$

4.2. Results for z = constant

A typical result is shown in Fig. 9. In order to correct for the influence of the diameter of the integrating sphere on the measured signal, we tried to

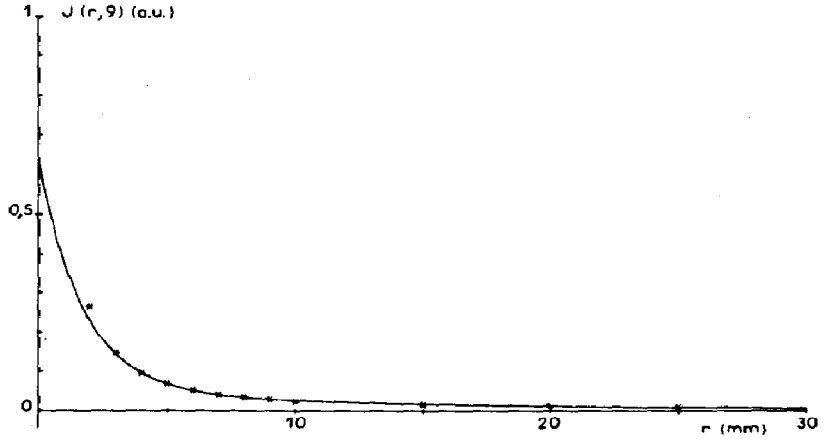

Fig. 9. Variation in the signal $J(r, 9)$ with r. The curve is calculated.

fit the measured data to monoexponential and bi-exponential functions in the range 4 mm $\leqslant r \leqslant$ 30 mm. The bi-exponential decay function

$$J(r, z) = A_1 \exp\left(-\frac{r}{\tau_1}\right) + A_2 \exp\left(-\frac{r}{\tau_2}\right) \tag{4}$$

represented exactly the data outside the fitting domain for $r > 2.5$ mm, whereas the monoexponential decay function showed only a good approximation to the data for which it had been optimized. According to the simulations, we therefore retained the bi-exponential function (Fig. 9). The ratio A_1/A_2 of the pre-exponential factors is usually about 10, whereas the corresponding ratio of constants τ_i is about 1/10.

A representation of the local light distribution as a function of z and r is given in Fig. 10. The intensity $J(0, z)$ can thus be separated into a direct part belonging to the incident beam and a scattered part which has already undergone scattering. Thus

$$J(0, z) = J(0, z)_{\text{dir}} + J(0, z)_{\text{dif}} \tag{5}$$

where $J(0, z)_{\text{dir}}$ and $J(0, z)_{\text{dif}}$ are the direct contribution and the scattered contribution respectively.

As Fig. 11 shows, the function $J(0, z)_{\text{dir}}$ (which has been obtained by subtraction of the extrapolated scattered values at $r = 0$ from the measured intensities at $r = 0$ (eqn. (5)) can itself be expressed as an exponential.

4.3. Scattered light contribution

It now seemed interesting to evaluate the function describing the proportion of scattered light relative to the total amount of light for the total reactor volume, and not only for $r = 0$. Equation (5) then becomes

$$I(z) = I(z)_{\text{dir}} + I(z)_{\text{dif}} \tag{6}$$

The direct and scattered contributions can be obtained by integration:

$$I(z) = 2\pi \left\{ \int_0^R \int_{z_1}^{z_2} J(0, z)_{\text{dir}} r \, dz \, dr + \int_{z_1}^{z_2} \int_0^{\infty} J(r, z)_{\text{dif}} r \, dr \, dz \right\} \tag{7}$$

In order to determine the ratio of the scattered light to the total amount of light, we consider the function

$$I(z)_{\text{dif}} = \int_{z_1}^{z_2} \int_0^{\infty} J(r, z)_{\text{dif}} r \, dr \, dz \Big/ I(z) \tag{8}$$

This function was found not to be constant because of the variation with z of $J(r, z)_{\text{dif}}$ itself, $J(r, z)_{\text{dif}}$ having been obtained for $z =$ constant, as explained in Section 4.2.

To overcome this problem we calculated the sum function of eqn. (8):

$$I(z)_{\Sigma} = \sum_{z=0}^{z} I(z) \tag{9}$$

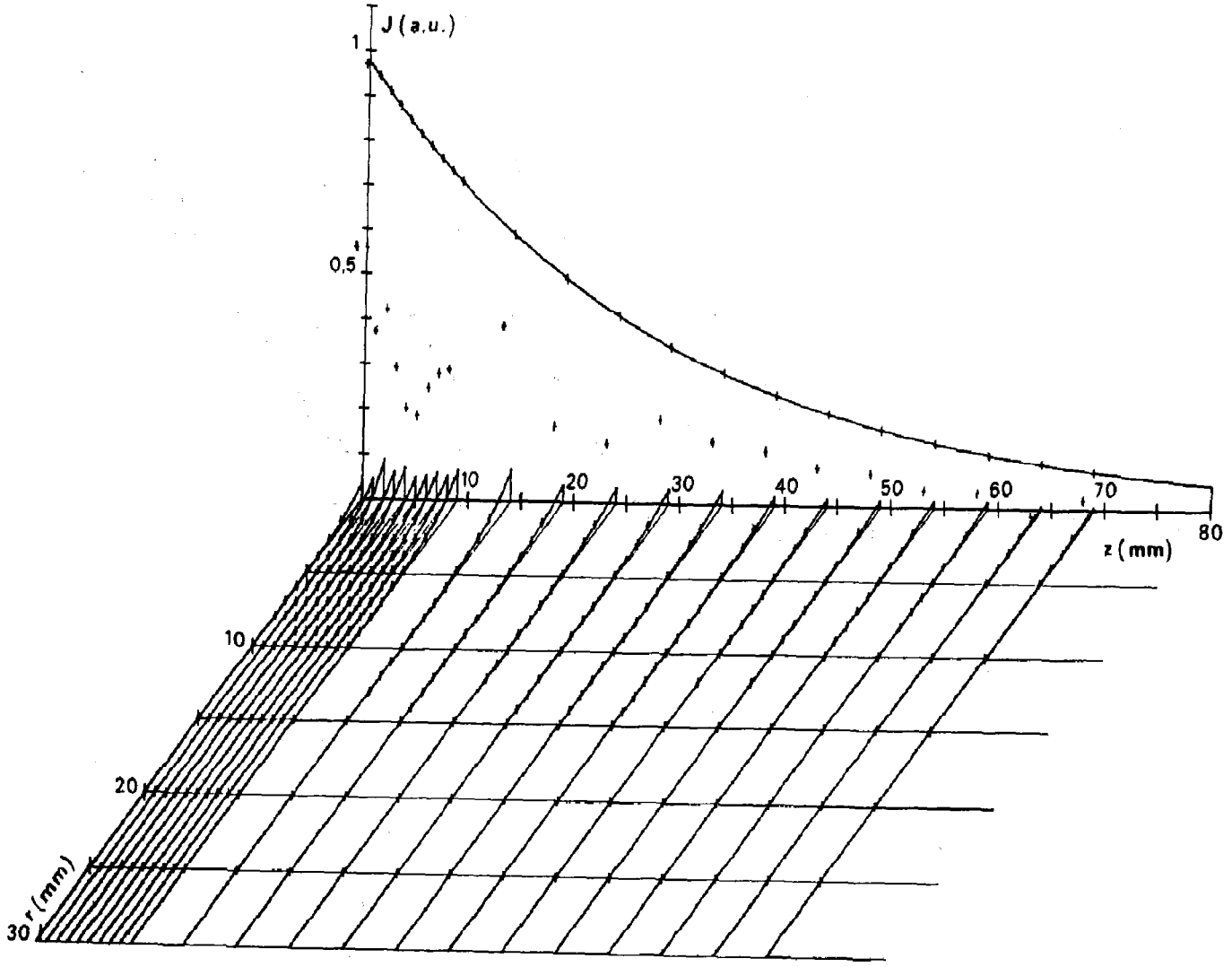

(a)

Fig. 10 *(continued).*

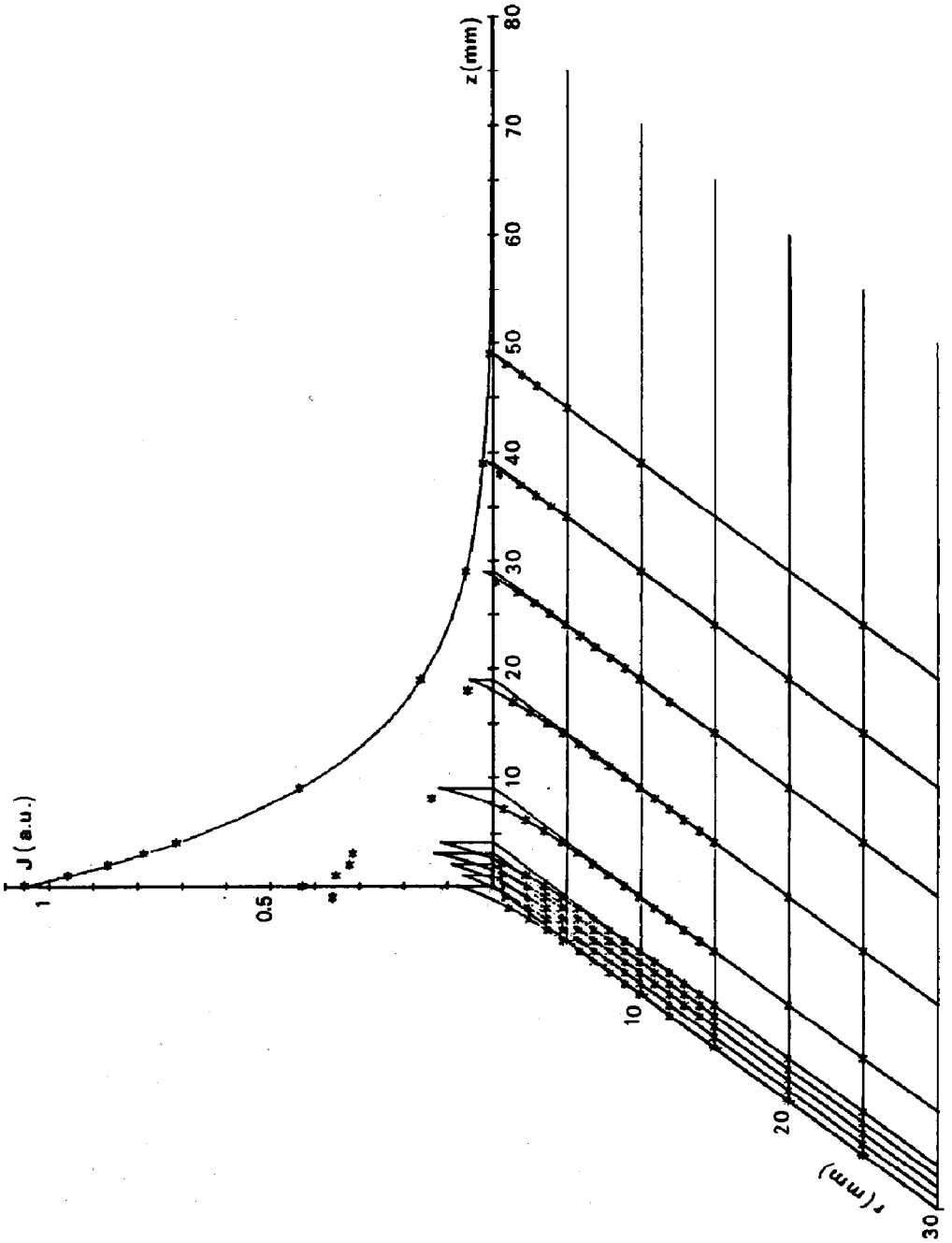

(b)

Fig. 10. Variations in J *vs.* r and z: (a) run 1; (b) run 5.

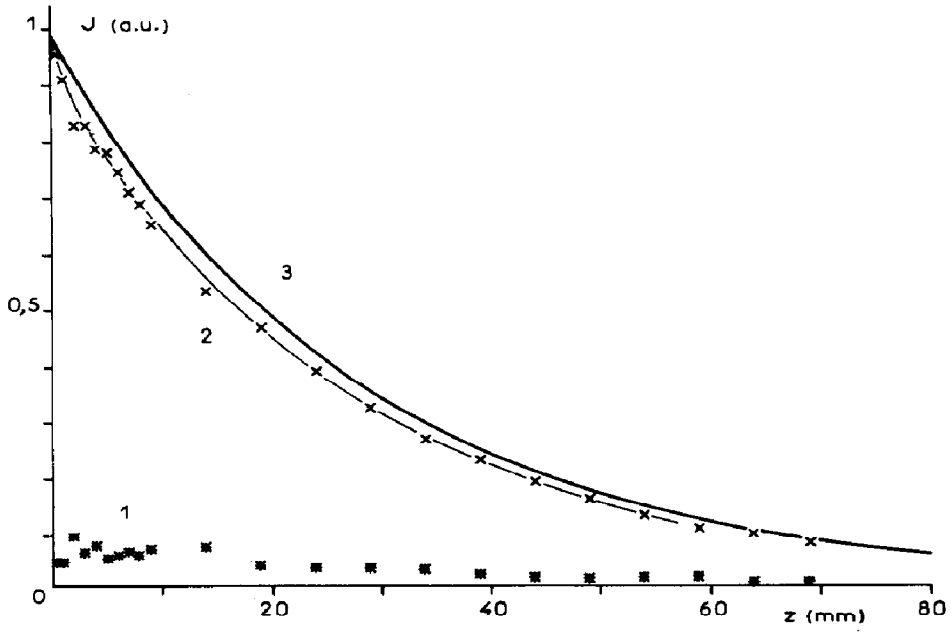

Fig. 11. Variation in $J(0, z)$ *vs.* z for run 1: curve 1, $J(0, z)$ calculated; curve 2, $J = J_{(3)} - J_{(1)}$; curve 3, $J(0, z)$ measured.

and could represent it by an exponential function with two adjustable parameters M and N (Table 1) with a good fit:

$$I(z)_\Sigma = M\{1 - \exp(-Nz)\} \tag{10}$$

We again obtained the desired function $I(z)$ by derivation:

$$I(z) = \frac{\mathrm{d}(I(z)_\Sigma{}^*)}{\mathrm{d}z} = MN \exp(-Nz)$$

With this new expression for $I(z)$ we could transform function (8) into

$$I(z)_{\mathrm{dif}} = \left\{MN \exp(-Nz) - \int_0^R \int_{z_1}^{z_2} J(0, z)_{\mathrm{dir}} r \, \mathrm{d}z \, \mathrm{d}r\right\} \Big/ MN \exp(-Nz)$$

This function, showing the contribution of the scattered light to the total light in the reactor, is shown in Fig. 12. It increases exponentially from already high values (27.5% at $z = 0$ for run 1) eventually to 100%. This was nearly attained by our measured values for run 5 with 99.5% at $z = 40$ mm.

4.4. Influence of the concentration on the light distribution in the reactor

$I(z)$, calculated in Section 4.3, is a very important function which describes the distribution of the exciting light averaged over r. It corresponds equally well to the local intensity when the incident light is of infinite cross section and of constant flux such as that given by the Sun under normal irradiation conditions. This result can be explained by the superposition of the effects of several "elementary" light beams such as laser beams with small cross sections.

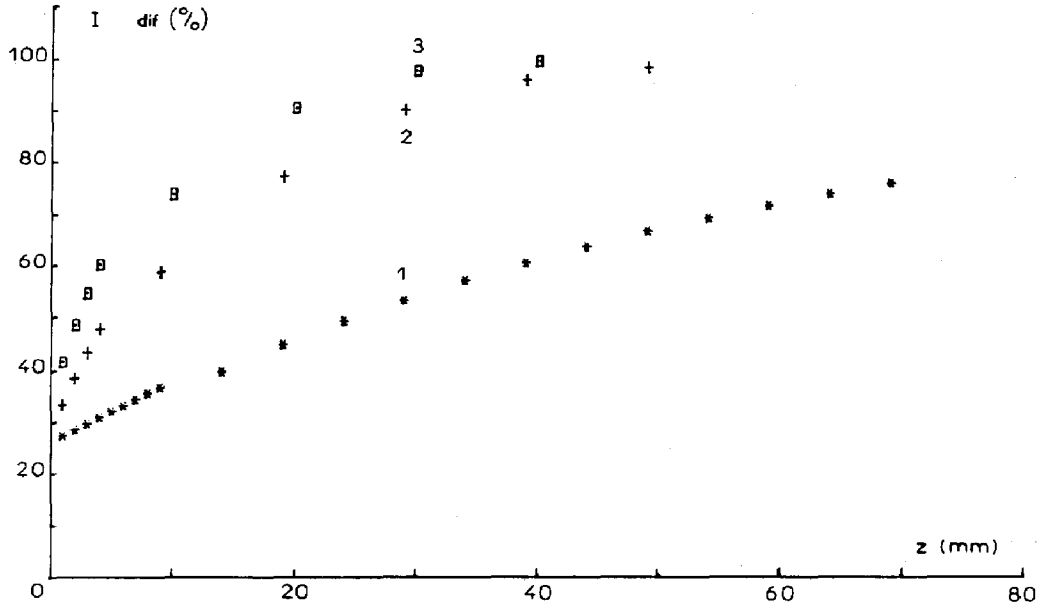

Fig. 12. Contribution of the scattered light to the total light in the reactor: curve 1, run 1; curve 2, run 3; curve 3, run 5.

Experimentally, we find that $I(z)$ can be represented by an expression similar in form to

$$I(z) = P \exp(-Nz)$$

where P and N are two adjustable parameters ($P = MN$).

For the three concentrations studied, N is found to be almost independent of c and corresponds to an apparent optical density of $N \times 10$ mm = 0.19 (Table 1). This result appears to be surprising at first glance as the visual experience of the experimentalist, who is in fact governed by an approximate knowledge of the backscattering, leads us to assume that, as the medium becomes more dense, there is more backscattering and consequently the optical density in the reactor is higher. In the calculations which we have shown here the flux at $z = 0$ corresponds in fact to the flux entering the reactor, *i.e.* it corresponds to the incident flux minus the flux of the backscattering. It is for this reason in particular that the optical density calculated by this method is always lower than that measured using a UV–visible absorption spectroscope even when we take the geometry of the measuring cell for which the reference flux is the incident flux into account.

4.5. Limits of the simulation and of the method

First of all, the apparatus used for this study does not allow us to examine situations where the scattering is too great because of the size of the integrating sphere placed at the end of the fibre. This is what happens in runs 4 and 5 where the modelling of $J(0, z)$ does not fit the experimental values very well.

For low concentrations we have made an assumption in the initial modellings carried out for random scattering ($P(\theta, \varphi) = 1$). By drawing contours in r, z space, we find that the results, *e.g.* in Fig. 13, correspond exactly to the experiment.

However, as is shown by the results in Fig. 14, which correspond to measurements carried out with the lowest concentrations of scattering

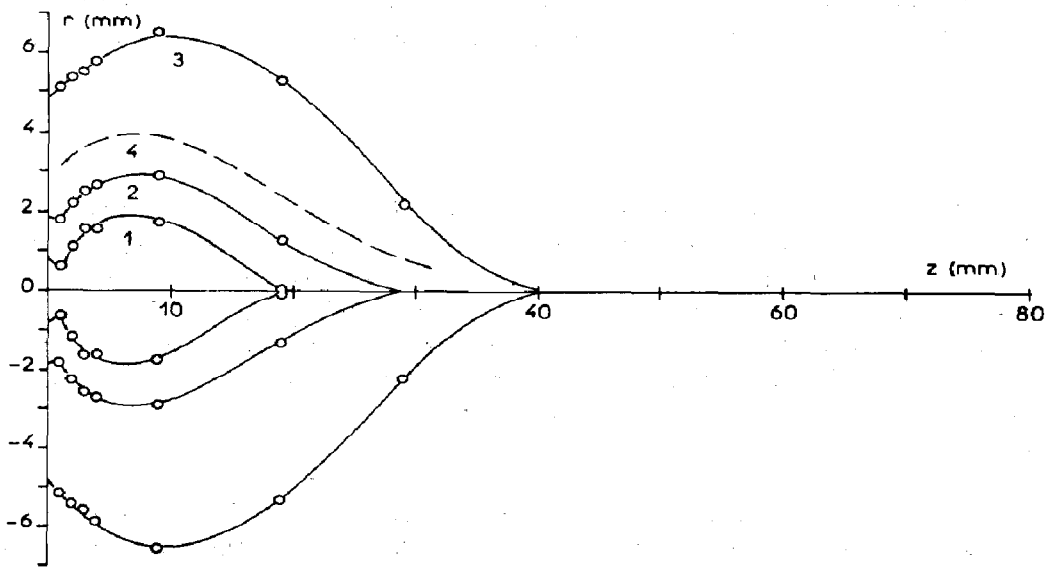

Fig. 13. Contours in r, z space of $J(r, z)$ for run 5: curve 1, $J(r, z)/J(0, 0) = 0.05$; curve 2, $J(r, z)/J(0, 0) = 0.03$; curve 3, $J(r, z)/J(0, 0) = 0.01$; curve 4, typical curve using Monte Carlo simulations.

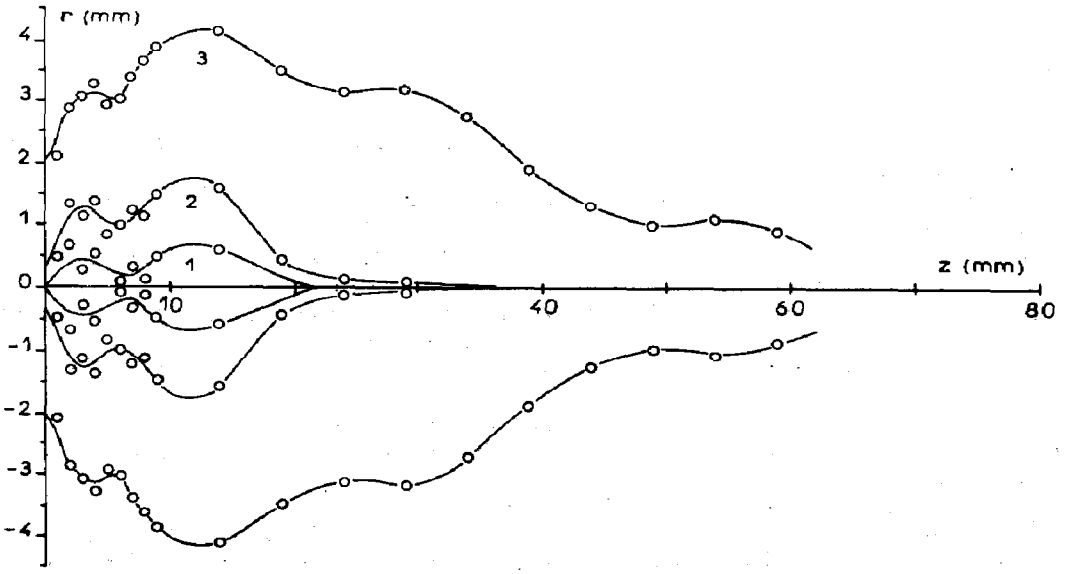

Fig. 14. Contours in r, z space of $J(r, z)$ for run 1: curve 1, $J(r, z)/J(0, 0) = 0.45$; curve 2, $J(r, z)/J(0, 0) = 0.25$; curve 3, $J(r, z)/J(0, 0) = 0.05$.

product, it is possible to show that the measurements differ from the simulation on the assumption that $P(\theta, \varphi) = 1$. Even the first values could be the result of experimental errors, this is not the case for the larger values of z where we observe fluctuations. As has been explained by Mills and Aufrere [6], this type of situation may correspond to non-uniformity of the scattering function.

Thus, this type of experiment allows us to demonstrate the existence of multiple scattering which does not correspond exactly to uniform scattering.

5. Conclusion

In this paper we have proposed a method for the study of the light distribution in a photoreactor when the exciting light is only scattered. Apart from the backscattering, which naturally increases with increases in the concentration of the scattering substance present in the solution, we show that it is possible to represent to a reasonably good approximation the law for the light distribution in such a system by a phenomenological expression of the same type as the Beer–Lambert law:

$$I(z) = I(0) \exp(-Nz)$$

where N is a constant and z is the depth. Experimentally, N is found to be almost independent of the scattering substance when no absorption process takes place.

This simple relationship is of great interest to us in the continuation of our work for cases where the particles of the photocatalyst play a dual role causing scattering and absorption to occur.

References

1 A. Tournier, X. Deglise, J. C. Andre and M. Niclause, *AIChE J.*, *28* (1982) 156, and references cited therein.
J. C. Andre, M. L. Viriot, J. Villermaux and A. Tournier, *Entropie*, *107 - 108* (1982) 62, and references cited therein.
J. Villermaux, J. C. Andre and M. Roger, *Proc. Conf. on Prospects in Industrial Photochemistry, Nancy, January 5, 1984*, in *Entropie*, to be published.

2 F. Cardon, W. P. Gomes and W. Oekeyser, *Photovoltaic and Photoelectrochemical Energy Conversion*, Plenum, New York, 1981, and references cited therein.
M. Grätzel and V. H. Houlding, *J. Am. Chem. Soc.*, *105* (1983) 5695, and references cited therein.
H. S. Wrighton, *Acc. Chem. Res.*, *12* (1979) 300, and references cited therein.
K. Honda, A. Fujishima and T. Miyasaka, *Kagaku (Kyoto) Zokan*, *86* (1980) 23, and references cited therein.

3 D. F. Ollis and A. L. Pruden, *Environ. Sci. Technol.*, *17* (1983) 628.

4 J. C. Ravey, in M. L. Viriot, J. C. Andre, M. Lucius and J. F. Stoltz (eds.), *Techniques Avancées en Hémorhéologie*, Département de Perfectionnement des Ingénieurs et Cadres–Institut National Polytechnique de Lorraine, Nancy, 1984, pp. 505 - 542.
H. C. van de Hulst, *Multiple Light Scattering*, Academic Press, New York, 1980.

5 D. Balland, R. Guillard and J. C. Andre, *Polym. Photochem.*, *4* (1984) 111.
6 P. Mills, *Rev. Phys. Appl.*, *15* (1980) 1357.
P. Mills and J. Aufrere, in M. L. Viriot, J. C. Andre, M. Lucius and J. F. Stoltz (eds.), *Techniques Avancées en Hémorhéologie*, Département de Perfectionnement des Ingénieurs et Cadres–Institut National Polytechnique de Lorraine, Nancy, 1984, pp. 543 - 579.

Appendix A: Nomenclature

A	pre-exponential factor of the function $J(0, z)$
A_1, A_2	pre-exponential factors of the function $J(r, z)$ with z = constant
B	exponential factor of the function $J(0, z)$
B_0	pre-exponential factor of the function $B(c)$
c	concentration (g l^{-1})
F	exponential factor of the function describing B
$I(z)$	function describing the total energy in the reactor as a function of z
$I(z)_{dif}$	part of the function $I(z)$ coming from the scattered light
$I(z)_{dir}$	part of the function $I(z)$ coming from the direct light
$I(z)_\Sigma$	function describing the total energy between $z = 0$ and z as a function of z
$J(r, z)$	function describing the local intensity as a function of r and z
$J(r, z)_{dif}$	part of the function $J(r, z)$ coming from the scattered light
$J(r, z)_{dir}$	part of the function $J(r, z)$ coming from the direct light
M	pre-exponential factor of the function $I(z)_\Sigma$
N	exponential factor of the function $I(z)_\Sigma$ and $I(z)$
p	probability of scattering
P	pre-exponential factor of the function $I(z)$
$P(\theta, \varphi)$	function of the probability of scattering as a function of the angles θ and φ
R	radius of the integrating sphere

Greek symbols

θ, φ	angles describing the path followed by a photon in space
τ_1, τ_2	lengths of relaxation of the function $J(r, z)$ with z = constant